Reactive and Functional Polymers 214 (2025) 106265

Contents lists available at ScienceDirect

Reactive and Functional Polymers

journal homepage: www.elsevier.com/locate/react

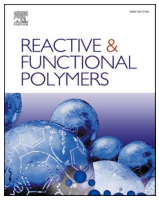

Simultaneous hypercrosslinking and functionalization of porous polystyrene adsorbent for protein-bound uraemic toxins removal

Lingyu Chen [a], Yunhong Liu [b,*], Xinyan Peng [b,*], Yuelan Wei [b], Ke Shao [c]

[a] College of Chemistry and Materials Science, Fujian Normal University, Fuzhou, Fujian 350117, China
[b] College of Chemical Engineering and Materials Science, Quanzhou Normal University, Quanzhou, Fujian 362000, China
[c] Jafron Biomedical Co., Ltd, Zhuhai, Guangdong 519085, China.

ARTICLE INFO

Keywords:
Protein-bound uraemic toxins
Hypercrosslinked adsorbent
Tertiary amine group
Blood compatibility
Hemoperfusion

ABSTRACT

Protein-bound uremic toxins (PBUTs) play a crucial role in the progression of uremic complications. Due to the extremely high binding affinity to human serum albumin, PBUTs are poorly removed by traditional hemodialysis methods. As an advanced blood purification technology, hemoperfusion has been proven effective in removing PBUTs, and hyper-crosslinked polystyrene adsorbents have been widely commercialized as hemoperfusion adsorption materials. However, challenges still remain, including the need to enhance the adsorption efficiency of PBUTs and the simplification of the preparation and modification processes of the adsorbents. In this work, we report a one-step external crosslinking modification technique to prepare a functionalized hyper-crosslinked polystyrene adsorbent named HCP-DFDA, in which *N*,*N*-dimethylformamide dimethyl acetal (DFDA) with tertiary amine functional groups was used as a small-molecule external crosslinker to simultaneously carry out Friedel–Crafts alkylation crosslinking and functional group grafting modification. Experimental results showed that the prepared hypercrosslinked resin HCP-DFDA had abundant mesoporous/microporous structures and an extremely high specific surface area of up to 1030 m^2/g. Adsorption experiments demonstrated that HCP-DFDA exhibited excellent adsorption performance for both uremic PBUTs like indoxyl sulfate (IS) and p-cresyl sulfate (PCS) and medium- to large-molecular-weight toxins such as β2-microglobulin (β2-MG) and interleukin-6 (IL-6). Moreover, similar to the commercial HA130 resin, HCP-DFDA exhibited low protein adsorption and hemolysis rates, demonstrating good blood compatibility. In summary, the facile preparation method of the modified hypercrosslinked adsorbent proposed in this study provides a new idea and solution for the efficient removal of PBUTs through whole-blood hemoperfusion in clinical applications.

1. Introduction

Protein-bound uremic toxins (PBUTs), such as indoxyl sulfate (IS) and p-cresyl sulfate (PCS), exhibit a strong binding affinity to plasma proteins. Consequently, the concentrations of their free forms in plasma are extremely low, which makes them difficult to be removed by traditional dialysis methods. Hemoperfusion, as an advanced blood purification technology, has been proven effective in removing PBUTs. Some porous materials for hemoperfusion that can selectively adsorb PBUTs have been reported, including activated carbon [1,2], zeolites [3–5], resins [6,7], metal-organic frameworks (MOFs) and MXenes [8–12]. For example, Yamamoto et al. found that using an extracorporeal circulation method with activated carbon adsorbents achieved an IS clearance rate of over 60 % [13]; Bruno et al. found that the clearance rates for PCS could reach 53 % by using an HDF system containing a micro-sized neutral resin adsorption column [14]. Although activated carbon and micro-sized neutral resins can effectively remove PBUTs, their insufficient blood compatibility prevent them from being applied in the whole blood perfusion modes. This will result in limited therapeutic effects and increased treatment costs, which is not conducive to clinical application. In recent years, some researchers have employed MOFs and other novel porous materials to remove PBUTs, achieving satisfactory results and demonstrating considerable application potential. However, these new materials are still in the experimental stage, and their safety, effectiveness, and economic costs remain to be evaluated and verified.

Hypercrosslinked macroporous polystyrene adsorbents, such as the HA resin of Jafron Biomedical Company, have high porosity, a large

* Corresponding authors at: College of Chemical Engineering and Materials Science, Quanzhou Normal University, Quanzhou, Fujian 362000, China.
E-mail addresses: liuyunhong@qztc.edu.cn (Y. Liu), pengxinyan@qztc.edu.cn (X. Peng).

https://doi.org/10.1016/j.reactfunctpolym.2025.106265
Received 22 December 2024; Received in revised form 12 March 2025; Accepted 12 March 2025
Available online 9 April 2025

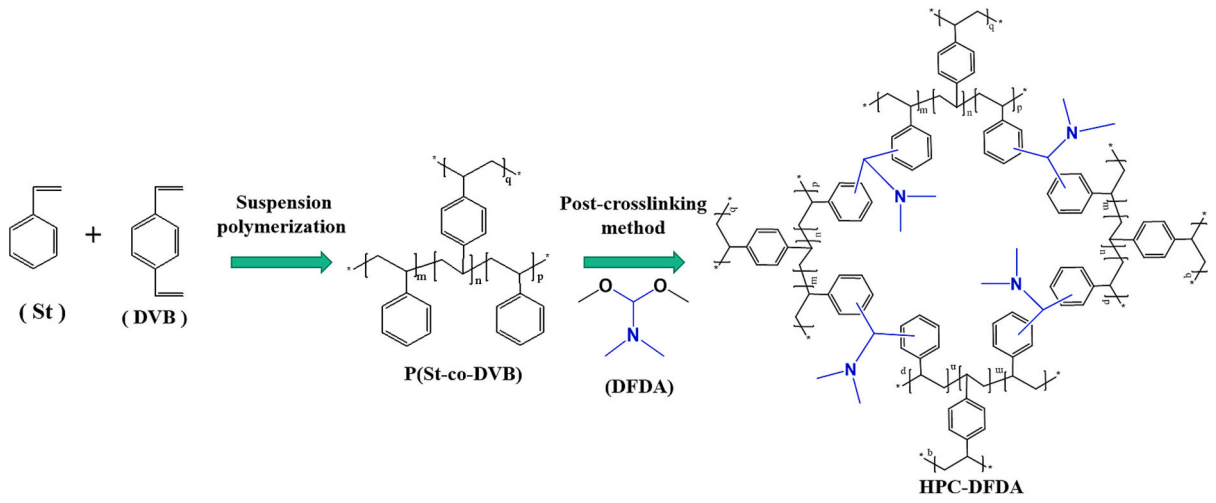

Fig. 1. Schematic diagram of the route to fabricate the HCP-DFDA.

specific surface area and good blood compatibility, enabling them to adsorb various blood toxins with high capacity, including small molecule toxins and medium- to large-molecular-weight substance [15], and have been widely used in whole-blood perfusion treatments for conditions such as uremia, critical cytokine storms, drug overdose, and acute poisoning [16,17]. However, these hypercrosslinked polystyrene adsorbents still face some problems, such as poor adsorption effect on PBUTs and the complexity of the material preparation and modification processes. The existing resins are synthesized using the classic Davankov method, which involves the chloromethylation of low-cross-linked polystyrene-divinylbenzene copolymer microspheres, followed by Friedel–Crafts post-crosslinking. The separation of the chloromethylation and post-crosslinking processes makes the preparation process too cumbersome and costly. In addition, reagents such as chloromethyl ether are highly toxic. Moreover, hypercrosslinked polystyrene resins usually remove small and medium- to large-molecular-weight toxins through the physical adsorption of their pore structures, but have a poor effect on the removal of PBUTs.

In recent years, scientists have explored various optimized preparation methods for hypercrosslinked polystyrene materials, such as the direct one-step polycondensation of the para-chloromethyl styrene method [18,19], pendent vinyl groups post-crosslinking [20,21], dichloroalkanes post-crosslinking [22], and direct external crosslinking method [23–25]. In order to improve the specific adsorption capacity of hypercrosslinked resins, functional modifications based on the properties of the target substances [26–28] (such as chemical functional groups, charges, etc.) are usually used, such as post-crosslinking followed by post-functionalization [29,30], pre-functionalization followed by post-crosslinking [31], and surface treatment techniques [32,33].

In our previous work, we prepared imidazole- and pyridine-functionalized hypercrosslinked polystyrene resins through a functional modification method, and the obtained adsorbents showed good removal efficiencies for IS, PCS, and bilirubin [34]. However, the functional modification inevitably leads to problems like a complicated preparation route, an extended production cycle, and increased costs. To address the issues of insufficient adsorption capacity of existing hemoperfusion hypercrosslinked adsorbent for PBUTs, as well as the complexity of the resin preparation and modification, this paper proposes a one-step method using small-molecule external cross-linking agents with tertiary amine functional groups to conduct Friedel–Crafts post-crosslinking reaction and functional group modification on pre-crosslinked polystyrene resins simultaneously. The adsorption performance of the adsorbent for PBUTs and medium- to large-molecular-weight toxins was studied, and the blood compatibility of the adsorbent was evaluated. As a new type of whole-blood perfusion adsorbent, this rein shows good application potential in the clinical treatment of uremia.

2. Experimental

2.1. Materials

Divinylbenzene (DVB, 80 % grade), styrene (St), benzoyl peroxide (BPO), methyl isobutyl carbinol (MIBC), 1,2-dichloroethane (DCE, AR grade), p-cresyl sulfate (PCS), phosphate-buffered saline (PBS, 0.01 M, pH 7.2–7.4) and bovine serum albumin (BSA, 66 kDa) were purchased from Macklin Ltd. (Shanghai, China). Indoxyl sulfate (IS) was purchased from Sigma-Aldrich (Shanghai, China). Sodium hydroxide (NaOH, AR grade), gelatine(99 %), absolute ethanol (GR grade), hydrochloric acid (HCl, 36.0–38.0 wt%, GR grade), anhydrous ferric chloride (AR grade), *N*,*N*-dimethylformamide dimethyl acetal (DFDA, 98 % grade) and trimethyl orthoformate (TMOF, 98 % grade) were all purchased from Aladdin Ltd. (Shanghai, China). Human serum was provided by blood bank in China. All reagents were used without further purification.

2.2. Preparation of porous polystyrene adsorbent

Firstly, pre-crosslinked polystyrene resin was synthesized via the suspension polymerization method. Subsequently, anhydrous ferric chloride was utilized as a catalyst, and *N*,*N*-dimethylformamide dimethyl acetal (DFDA) functioned as a functional small-molecule external crosslinker to conduct the post-crosslinking reaction of the pre-crosslinked polystyrene resin. The schematic illustration of the preparation process is presented in Fig. 1.

2.2.1. Synthesis of pre-crosslinked polystyrene resin

The pre-crosslinked polystyrene resin was synthesized via the suspension polymerization method. The aqueous phase was prepared as follows: 200 g of deionized water and 4 g of gelatine were blended under agitation at 55 °C until complete dissolution. Subsequently, the monomers (30 g of St and 6 g of DVB), porogens (17 g of toluene and 38 g of MIBC) and the initiator (0.5 g of BPO) were dissolved at room temperature to prepare the organic phase. This two-phase mixture was then introduced into the reactor and polymerized at 75–85 °C for 12 h. After the reaction was completed, the mixture was cooled to room temperature, and the resulting adsorbent was washed successively with pure water and edible alcohol. The obtained pre-crosslinked polystyrene resin was designated as P(St-co-DVB).

2.2.2. Preparation of hypercrosslinked polystyrene adsorbents

P(St-co-DVB) (11 g) was swollen in 1,2-dichloroethane (1,2-DCE) (160 mL) for 12 h, and then DFDA (12 g) and $FeCl_3$ catalyst (60 g) were added to the reaction mixture successively. The mixture was stirred at 50 °C for 5 h, followed by heating to 80 °C and maintaining the reaction for 5 h. Subsequently, the reaction mixture was washed with ethanol until the filtrate was clear. The synthesized adsorbents were washed with 0.5 M aqueous HCl solution, followed by rinsing with distilled water until the pH of the rinse solution reached neutrality. Subsequently, the resin was treated with 0.5 M aqueous NaOH solution and further rinsed with deionized water until a neutral pH was attained. Thereafter, the product was extracted with ethanol in a Soxhlet extractor for 12 h and then dried in a vacuum oven at 80 °C for 5 h. The resultant porous HCPS were designated as HCP-DFDA. Additionally, following a similar preparation process as described above, trimethyl orthoformate (TMOF) was used as a small molecular crosslinking agent, and the obtained hypercrosslinked adsorbent was denoted as HCP-TMOF.

2.3. Measurements

The morphology of the adsorbents was investigated using a Merlin compact scanning electron microscope (SEM) (Carl Zeiss, Germany). N_2 sorption isotherms were measured by a porosity analyzer (BSD-660MG) at −196 °C. Approximately 160 mg of the samples were degassed at 90 °C under vacuum (0.003 mbar) overnight prior to the measurement. The Brunauer-Emmett-Teller (BET) method was applied to determine the surface area. The FTIR spectra of the samples were acquired in the range of 400–4000 cm^{-1} with a resolution of 2 cm^{-1} and were recorded by an ATR-FTIR spectrometer (Nicolet iS50 Thermo Scientific, Waltham, MA, USA). The surface chemistry of the samples was analyzed by X-ray photoelectron spectroscopy (XPS). The XPS measurements were carried out using a PHI VersaProbe II spectrometer (ULVAC-PHI, Inc., Kanagawa, Japan) equipped with a monochromatic Al Kα X-ray source operating at a spot size of 100 μm. The Nitrogen content of the adsorbents was measured using an Elementar Unicube elemental analyzer (EA; Germany).

2.4. Adsorption assays in a bovine serum albumin (BSA) solution

PBUTs/BSA buffer solution was prepared by dissolving PCS in a PBS buffer solution with the presence of 40 gL^{-1} BSA. The initial concentration of PCS was set at 25.0 mg L^{-1}. A total volume of 5.0 mL of the adsorbent (wet volume) was added to 50 mL of the PBUTs/BSA solution at 37 °C. After being shaken at 140 rpm for a specific period of time, 0.50 mL of the solution was taken out. Subsequently, 0.5 mL of acetonitrile was added to the withdrawn solution to precipitate the BSA and to completely dissociate the PBUT from the BSA. The resulting mixture was then vortex-mixed for 30 s and centrifuged at 3000 rpm for 10 min. The concentration of PBUTs in the supernatant was determined using a fluorescence spectrophotometer. The removal rates of PBUTs at time t were calculated according to Eq. (1):

$$\text{PBUTs adsorption rate}(\%) = \left[\frac{(C_{0,PBUTs} - C_{t,PBUTs})}{C_{0,PBUTs}}\right] \times 100\% \quad (1)$$

where $C_{0,PBUT}$ (gL^{-1} is the initial PBUTs concentration and $C_{t,PBUT}$ (gL^{-1}) is the residual PBUTs concentration at time t.

2.5. Recyclability and stability tests of HCP-DFDA

The recyclability of HCP-DFDA was explored through an adsorption-regeneration procedure. 6.0 g of HCP-DFDA was placed into a 500-mL conical flask, and 100.0 mL of a PCS-PBS solution with an initial concentration of 100.0 mg L^{-1} was added. The mixture was placed in a thermostatic oscillator and reacted continuously at 298 K with an oscillation speed of 120 rpm for 12 h to achieve adsorption equilibrium. After the reaction, the HCP-DFDA having adsorbed the target substances was was collected. The collected HCP-DFDA was subjected to desorption and regeneration treatment using a 0.1 M sodium hydroxide solution, and then washed three times successively with deionized water and absolute ethanol to remove surface-residual impurities. To investigate the recyclability of the material, a total of 5 consecutive adsorption - desorption cycle tests were carried out in this experiment. The regenerated material after each cycle was characterized for its adsorption performance according to the method described in Section 2.4.

To evaluate the chemical stability of HCP-DFDA, the samples were treated under the following three different conditions: (1) Immersion in an aqueous HCl solution (pH = 1.0); (2) Immersion in an aqueous NaOH solution (pH = 13.0); (3) Hydrothermal aging treatment at 60 °C. In all treatment processes, the liquid-to-solid ratio was maintained at 20 mLg^{-1} (volume-to-mass ratio), and static treatment was carried out for 72 h. The treated samples were thoroughly washed with deionized water and dried for 12 h. The regenerated adsorbent after each treatment was characterized for its adsorption performance according to the method described in Section 2.4.

2.6. Adsorption of uremic toxins in human plasma

PCS and IS were dissolved in human plasma with an initial concentration of 25.0 mg L^{-1}. A total volume of 1.0 mL (wet volume) of the adsorbents was introduced into a glass bottle containing 10.0 mL of the IS/PCS human plasma solution. The system was maintained at 37 °C and continuously shaken at 140 rpm for 2 h. After that, 0.5 mL of the solution was withdrawn, and 0.5 mL of acetonitrile was added to precipitate the human plasma. The resulting mixture was vortex-mixed for 30 s and then centrifuged at 4000 rpm for 10 min. The concentration of PBUTs was measured via high-performance liquid chromatography (HPLC) at 277 nm (IS) and 280 nm (PCS). The removal rate of PBUTs was calculated according to Eq. (2):

$$\text{Adsorption rate}(\%) = \frac{C_{blank} - C_s}{C_{blank}} \times 100\% \quad (2)$$

where C_S and C_{blank} are the PBUTs concentrations after adsorption with and without the adsorbents, respectively.

Similarly, the adsorption capacities towards medium- to large-molecular-weight toxins (e.g., PTH, β2-MG, and IL-6) were also investigated. The initial concentrations of i-PTH, β2-MG, and IL-6 dissolved in human plasma were 180 pmol L^{-1}, 5 mg L^{-1}, and 300 pg mL^{-1}, respectively. The concentrations of PTH, β2-MG, and IL-6 in human plasma were detected using an electrochemiluminescence immunoassay and a chemiluminescence method, respectively, by the testing services provided by Guangzhou King Med Diagnostics Group Co., Ltd. In the same vein, the adsorption capacities for albumin and total protein were also studied.

2.7. Adsorption kinetics of HCP-DFDA

To investigate the adsorption kinetics of PBUT on HCP-DFDA, 900 mg of HCP-DFDA was was added to 300 mL of a PBUTs/PBS solution (100 mg L^{-1}). The mixture was then shaken at 37 °C at a rotation speed of 115 rpm. At pre-determined time points (30, 60, 90, 120, 180, 240, 300, 420, 540, and 720 min), the concentration of residual PBUTs in the supernatant was measured using a fluorescence spectrophotometer.

The PBUTs adsorption capacity at time t (qt) was calculated via the following Eq. (3):

$$q_t = \frac{(C_0 - C_t) \times V}{m} \quad (3)$$

where q_t (mgg^{-1}) represents the amount of PBUTs adsorbed per unit mass of HCP-DFDA at time t; C_0 (mg L^{-1}) denotes the initial concentration of PBUTs; C_t (mg L^{-1}) indicates the concentration of residual PBUTs at time

t; V (mL) represents the volume of the solution; and m (g) represents the mass of HCP-DFDA employed in the adsorption process.

2.8. Adsorption isotherms of HCP-DFDA

Approximately 30 mg of HCP-DFDA and 20 mL of PBUTs/PBS aqueous mixture were introduced into the conical flasks. Isotherms at three different temperatures (298 K, 303 K, and 310 K) were collected for various initial concentrations of PCS/IS. The initial concentrations of PCS/IS were set at 200, 400, 600, 800 and 1000 mg L^{-1}. The flasks were then continuously shaken for 12 h at 37 °C and 115 rpm to reach equilibrium adsorption. The equilibrium PBUTs adsorption capacity (q_e) was calculated according to Eq. (4):

$$q_e = \frac{(C_0\text{-}C_e) \times V}{m} \quad (4)$$

where C_0 (mg L^{-1}) and C_e (mg L^{-1}) are the initial and equilibrium concentrations of PBUTs, respectively; V (mL) is the volume of the solution; and m (g) is the mass of HCP-DFDA employed in the adsorption process.

2.9. Blood compatibility assays

2.9.1. Haemolysis assay

A diluted rabbit blood suspension was prepared by combining 8.0 mL of fresh rabbit whole blood with 10.0 mL of phosphate-buffered saline (PBS) solution. The procedure of the haemolysis test was as follows: (1) 0.2 mL of the diluted blood suspension was mixed with 10 mL of deionized water to serve as a positive control, which was anticipated to induce 100 % haemolysis. (2) 0.2 mL of the diluted blood suspension was blended with 10 mL of PBS solution to act as a negative control, for which no haemolysis was expected to occur. (3) 0.2 mL of the diluted blood suspension was mixed with the tested adsorbent suspensions. In this case, 50.0 mg of the adsorbents were immersed in 10.0 mL of PBS. After being completely mixed, the samples were centrifuged at 4000 rpm for 5 min to separate the haemoglobin released from the lysed red blood cells. The absorbance (A) of the haemoglobin in the supernatant was measured using a LAMBDA 465 UV/vis spectrophotometer at a wavelength of 545 nm. The haemolysis ratio was calculated according to Eq. (5):

$$\text{Hemolysis ratio} = \frac{A_s - A_{NC}}{A_{PC} - A_{NC}} \times 100\% \quad (5)$$

where A_S, A_{NC}, and A_{PC} are the absorbances of the supernatants from the tested sample, the negative control (PBS solution), and the positive control (deionized water), respectively.

2.9.2. Recalcification time measurement

The blood recalcification time was measured to evaluate the anticoagulant performance of the adsorbents, and the specific details of the experimental procedure have been reported in our previous work [34]. In brief, 0.6 mL of fresh platelet-rich plasma (PRP) was added to the absorbents (0.3 mL), which had been immersed in PBS overnight. After an adequate incubation period, 100 μL of a 0.2 M $CaCl_2$ solution (at 37 °C) was added to each sample. The time interval from the start of adding calcium chloride to the point when the plasma was completely coagulated was defined as the recalcification time of the adsorbents.

3. Results and discussion

3.1. Structural characterization of the adsorbents

In this study, a hypercrosslinked adsorbent bearing tertiary amine functional groups, designated as HCP-DFDA, was synthesized via a one-step approach. Using DFDA, which contains tertiary amine groups, as a small-molecule external crosslinker, the Friedel–Crafts post-crosslinking reaction and functional group grafting modification were simultaneously carried out on the pre-crosslinked polystyrene resin. For the purpose of comparison, another small-molecule external crosslinker without functional groups, TMOF, was employed to prepare a control sample named HCP-TMOF following a similar procedure. Fig. 2 displays the FTIR spectra of P(St-co-DVB), HCP-DFDA, and HCP-TMOF. The peaks at 1450, 1491, and 1600 cm^{-1} can be assigned to the unsaturated C=C stretching vibration of the aromatic ring [35], and the peaks in the range of 3100 to 3000 cm^{-1} are attributed to the = C–H stretching vibration of benzene rings. When compared with P(St-co-DVB), two new and distinct peaks emerge on the curves of HCP-DFDA and HCP-TMOF at 1700 cm^{-1} and 3400 cm^{-1}, corresponding to the C=O and –OH groups, respectively. The presence of C=O and –OH groups may be associated with the hydrolysis side reactions of the methoxy groups in the small-molecule external crosslinkers during the crosslinking process, as well as the oxidation of the crosslinked structures between phenyl groups into oxygen-containing groups. Moreover, the HCP-DFDA adsorbent exhibits a characteristic peak at approximately 1356 cm^{-1}, which is attributed to the stretching vibration of C–N [36] in the tertiary amino groups. This indicated that through the post-crosslinking reaction, tertiary amine functional groups have been successfully grafted onto the structure of the adsorbents.

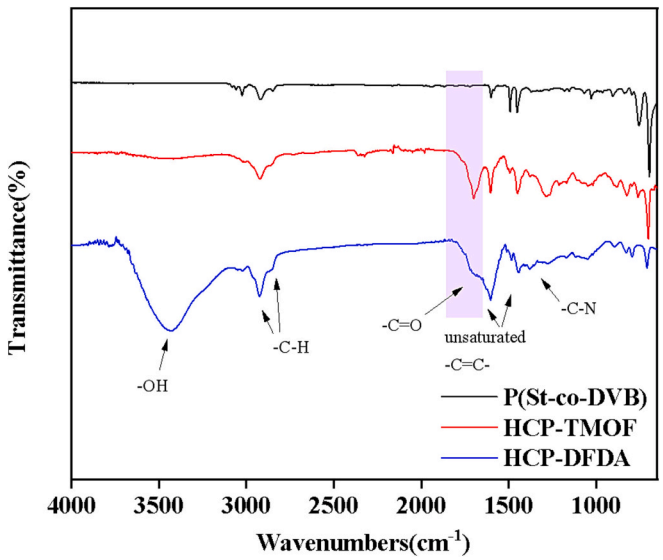

Fig. 2. FTIR spectra of P (St-co-DVB), HCP-TMOF and HCP-DFDA.

XPS was further utilized to analyze the elemental states of the synthesized adsorbents. As shown in Fig. 3(a), in contrast to P(St-co-DVB), the HCP-DFDA sample exhibites distinct N_{1s} and O_{1s} peaks, and their high-resolution spectra are shown in Fig. 3(b-d), respectively. From the high-resolution N_{1s} spectra in Fig. 3(b), a noticeable peak at 399.8 eV, which corresponded to the nitrogen in tertiary amine groups, is observed in the spectra of HCP-DFDA. This observation confirmed that tertiary amine groups had been successfully incorporated into the structure of the adsorbent through the post-crosslinking reaction. As shown in Fig. 3 (c) and Fig. 3(d), the high-resolution XPS spectra of O_{1s} for HCP-DFDA and HCP-TMOF can be deconvolved into three peaks at 531.4, 532.6, and 534.1 eV, which are attributed to C=O, C–OH, and C–O–C, respectively [37]. These results are in accordance with the aforementioned FTIR analysis, further confirming that the post-crosslinking reaction with small-molecule crosslinkers had introduced oxygen-containing chemical functional groups, such as hydroxyl and carbonyl groups, into the chemical structure of the hypercrosslinked adsorbents.

To more accurately and quantitatively analyze the chemical structures of the prepared adsorbents, the elemental compositions and ion exchange capacities of the adsorbents were measured, and the results

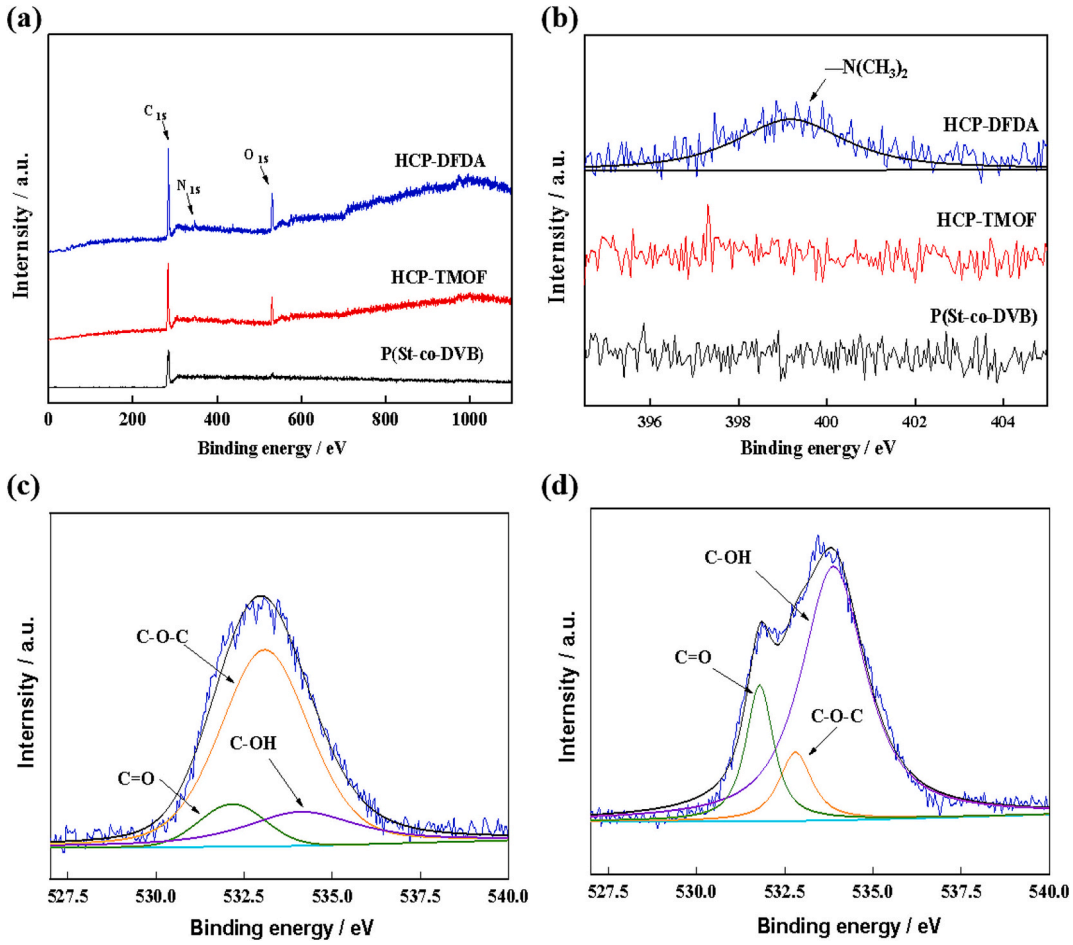

Fig. 3. (a) XPS survey spectra of the samples; (b) the magnified image around the N_{1s} region, and (c-d) O_{1s} XPS spectra of HCP-TMOF and HCP-DFDA.

Fig. 4. Optical images of (a) P(St-co-DVB), (b) HCP-TMOF and (c) HCP-DFDA.

are shown in Table S1. From the elemental analysis results, it can be seen that the contents of N, C, and H elements in the HCP-DFDA adsorbent were 0.15 %, 80.00 %, and 6.89 %, respectively. In contrast, no N element was detected in the HCP-TMOF adsorbent. Instead, the contents of carbon and hydrogen in HCP-TMOF were 86.83 % and 7.00 %, respectively. The maximum ion exchange capacities of HCP - DFDA and HCP-TMOF were 0.142 $mmol{\cdot}mL^{-1}$ and 0.015 $mmol{\cdot}mL^{-1}$, respectively, demonstrating a significant difference between the two. The above-mentioned quantitative results further confirmed that tertiary amine groups were grafted onto the HCP - DFDA adsorbent.

Fig. 4 displays the optical photographs of the P(St-co-DVB), HCP-TMOF, and HCP-DFDA adsorbents. As shown in Fig. 4(a), the precursor P(St-co-DVB) exhibites a regular spherical shape and a smooth surface, with a diameter ranging from 0.4 to 1.0 mm. After the post-crosslinking process, regardless of the crosslinking agent employed, there is no significant alteration in the particle size, shape, or surface roughness (Fig. 4 (b, c)). The precursor P(St-co-DVB) resin is white in color. However, upon the completion of the crosslinking process, their color transform into brown. The observed darkening of the HCP-TMOF and HCP-DFDA samples can be ascribed to the side reactions that took place under high temperatures and were catalyzed by ferric chloride. These reactions entailed the condensation and dehydrogenation of the benzene rings on the crosslinked polystyrene chains, resulting in the formation of conjugated π-electron systems. Such systems generated chromophores that absorbed visible light, thereby intensifying the color of the adsorbents [38].

The microstructures of the adsorbents were examined by scanning electron microscopy (SEM), as shown in Fig. 5. The images successively present the micromorphology of the external surfaces and internal structures of the adsorbents. As shown in Fig. 5(a_1–c_1), at low magnification, the external surfaces of all the samples are flat and smooth, with minimal defects. The inset images in the upper right corners of Fig. 5 (a_1–c_1) reveal the mechanical stability of the resin. When the pre-crosslinked resin P(St-co-DVB) sample was manually compressed with

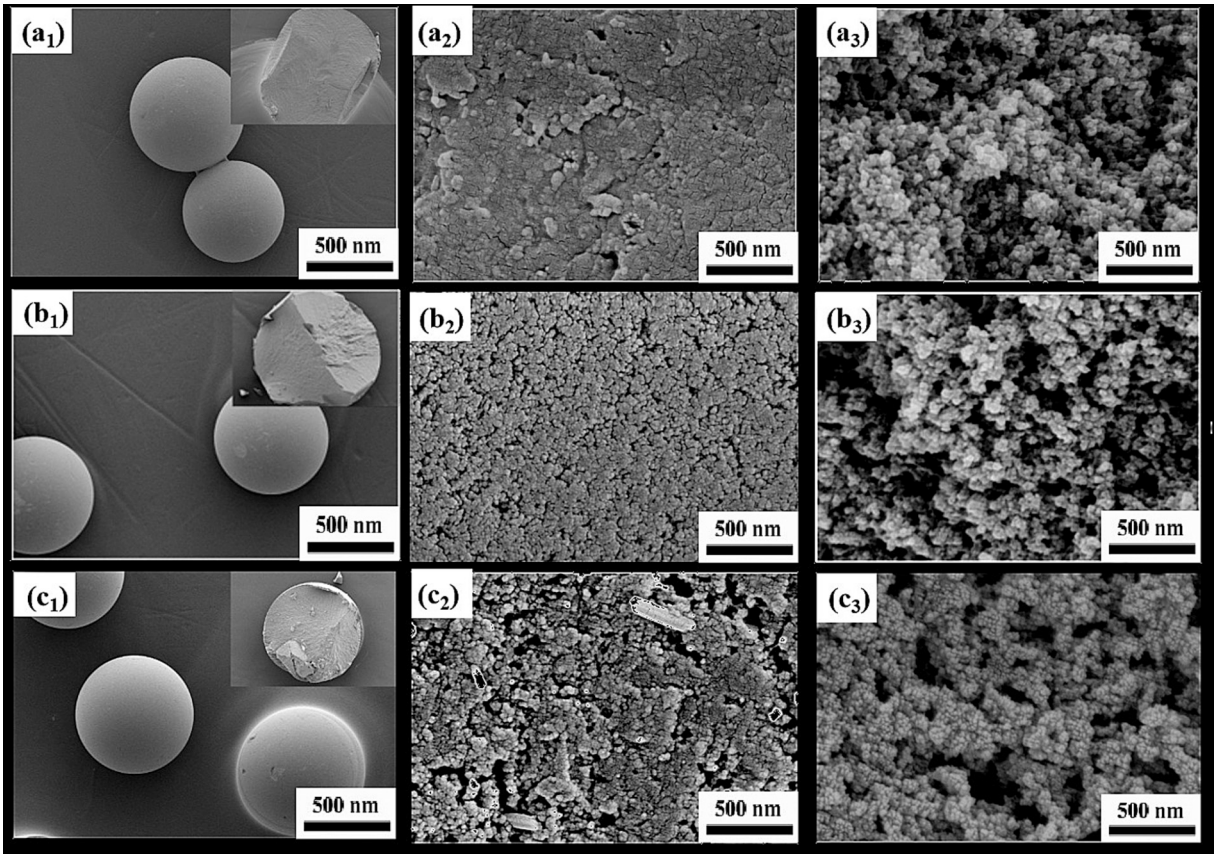

Fig. 5. The external surface and cross-sectional surface images of (a_1-a_3) P(St-co-DVB), (b_1-b_3) HCP-TMOF, and (c_1-c_3) HCP-DFDA beads.

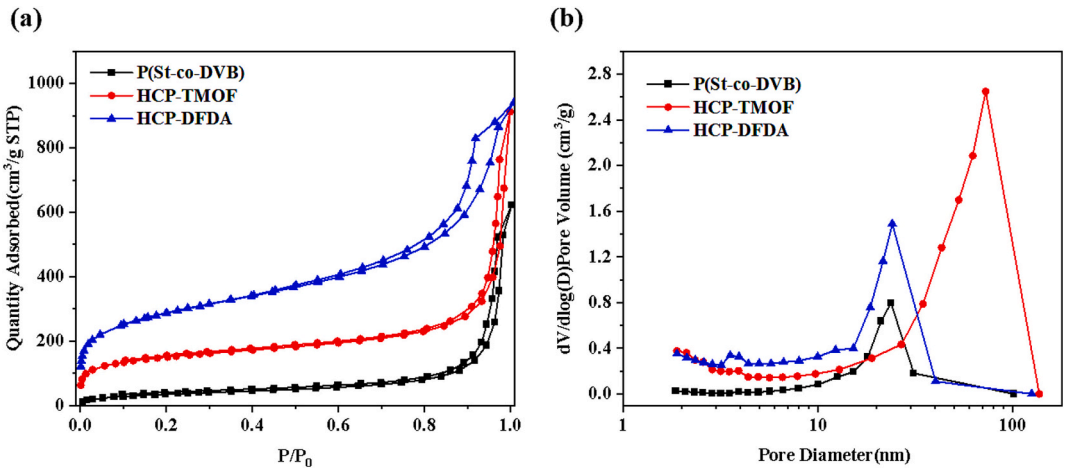

Fig. 6. (a) N_2 adsorption-desorption isotherms and (b) pore size distributions (PSDs) of P (St-co-DVB), HCP-TMOF and HCP-DFDA.

metal tweezers, it underwent substantial deformation before fracturing. Conversely, the post-crosslinked HCP-TMOF and HCP-DFDA samples demonstrated superior mechanical strength and stiffness, showing no obvious deformation under the applied force and fracturing abruptly in a brittle manner. From the SEM images of the material surfaces in Fig. 5 (a_2–c_2), distinct pore structures are observed on the surface of HCP-DFDA. In the cross-sectional images (Fig. 5(a_3–c_3), all the samples display apparent continuous accumulation of aggregated microstructures internally, with a specific distribution of pore structures between the aggregates. This was mainly attributed to the micro-phase separation between the porogen and the crosslinked polymer chains during the polymerization reaction. After the post-crosslinking process, the porous structures of HCP-TMOF and HCP-DFDA became more pronounced compared to those of P(St-co-DVB).

The alterations in the porous structure of the adsorbents before and after the post-crosslinking reaction were analyzed through N_2 gas adsorption-desorption isotherms. As illustrated in Fig. 6(a), at relative pressures (P/P_o) greater than 0.9, all the products manifest a rapid increase in the slopes of their isotherms and present hysteresis loops resulting from the divergence between adsorption and desorption branches. This phenomenon suggest the existence of mesoporous and macroporous structures within the materials. In the low-pressure region ($P/P_o < 0.1$), when compared with P(St-co-DVB), the post-crosslinked adsorbents HCP-DFDA and HCP-TMOF demonstrat notably enhanced

Table 1
Textural properties of the P(St-co-DVB), HCP-TMOF and HCP-DFDA samples.

Samples	S_{BET}[a] (m^2/g)	S^b_{micro} (m^2/g)	V^c_p (cm^3/g)	V^b_{micro} (cm^3/g)	Average pore size[d](nm)
P(St-co-DVB)	101.94	0	0.52	0	20.45
HCP-TMOF	543.06	338.02	1.18	0.23	8.71
HCP-DFDA	1030.13	476.14	1.40	0.43	5.42

[a] Values were calculated using the Brunauer-Emmett-Eller (BET) multi-point method. [b] Micropore volume/area with d<2 nm was calculated using the T-Plot method. [c] Calculated at the relative pressure of 0.99. [d] Calculated using the BJH model.

N_2 adsorption capacity, indicating the formation of numerous microporous structures after post-crosslinking. According to the International Union of Pure and Applied Chemistry (IUPAC) classification, HCP-DFDA and HCP-TMOF conform to Type IV isotherms [39]. The acquired pore size distribution (PSD) curves based on the Kelvin equation [40] depicted in Fig. 6(b) reveal that all three samples have a significant pore volume in the macroporous region (10–100 nm). In contrast to P(St-co-DVB), HCP-DFDA and HCP-TMOF samples exhibit a considerably higher proportion of pores within the 0–10 nm range. This finding is consistent with the pore structure analysis presented in Fig. 6(a), thereby confirming that the post-crosslinking process endowed HCP-DFDA and HCP-TMOF with a hierarchical pore structure comprising micropores, mesopores, and macropores.

The textural parameters of the samples were further investigated through BET analysis, and the findings were summarized in Table 1. It is evident that the P(St-co-DVB) sample had a specific surface area of only 101.94 m^2/g, with neither a measurable microporous surface area nor pore volume. After post-crosslinking, substantial alterations occurred in the pore structure parameters of HCP-DFDA and HCP-TMOF. Firstly, their specific surface areas increased to 1030.13 m^2/g and 543.06 m^2/g, respectively. Both HCP-DFDA and HCP-TMOF exhibited remarkable microporous characteristics, with microporous specific surface areas of 476.14 m^2/g and 338.02 m^2/g, and microporous pore volumes of 0.43 cm^3/g and 0.23 cm^3/g, respectively. Furthermore, the average pore size of HCP-DFDA and HCP-TMOFwere 5.42 nm and 8.81 nm, respectively, which were smallerr than that of P(St-co-DVB) (20.45 nm). The post-crosslinking reactions on the pre-crosslinked resin P(St-co-DVB) introduced additional crosslinking points into its structure, triggering the crosslinking and spatial rearrangement of molecular segments within the pre-crosslinked resin. As a result, a greater number of microporous structures were formed, directly contributing to an increase in the specific surface area and a decrease in the average pore size.

Notably, as presented in Table 1, HCP-TMOF exhibited much lower specific surface area and pore volume compared to HCP-DFDA. This discrepancy can be attributed to differential crosslinking behaviors during Friedel–Crafts alkylation, dictated by TMOF and DFDA, two small molecule crosslinking agents with different chemical structures. We conclude that DFDA exhibited superior crosslinking efficacy compared to TMOF, leading to a higher degree of network crosslinking. As crosslinking density increases, the resin network becomes more rigid and stable, effectively preserving the porogen-induced pore architecture. Elevated crosslinking density also strengthens intermolecular interactions between the polymer matrix and porogen molecules, such as hydrogen bonding and van der Waals forces, leading to more homogeneous porogen distribution. After porogen removal, this results in pores with narrower size distributions and improved structural uniformity, which collectively enhance both pore volume and specific surface area.

In this research, hypercrosslinked polystyrene adsorbents, namely HCP-DFDA and HCP-TMOF, were synthesized based on the mechanism of Friedel–Crafts alkylation reactions. Ferric chloride ($FeCl_3$) was employed as the catalyst, and DFDA and TMOF served as small-molecule external crosslinking agents. Taking DFDA as an illustration, the ferric chloride catalyst coordinated with the DFDA crosslinking agent to generate an electrophilic carbocation. This carbocation then underwent an electrophilic aromatic substitution reaction with the aromatic rings in the structure of the pre-crosslinked resin P(St-co-DVB), resulting in the formation of methylene bridge structures containing tertiary amine groups. This approach avoided the complex and time-consuming procedures involved in the traditional synthesis of hypercrosslinked polystyrene adsorbents. Furthermore, small-molecule external crosslinkers with functional groups (such as DFDA) enabled functional-group modification of the adsorbent. This was anticipated to endow the adsorbent with enhanced specificity and adsorption efficiency, thereby facilitating the advancement and practical application of hypercrosslinked polystyrene adsorbents in the field of hemoperfusion.

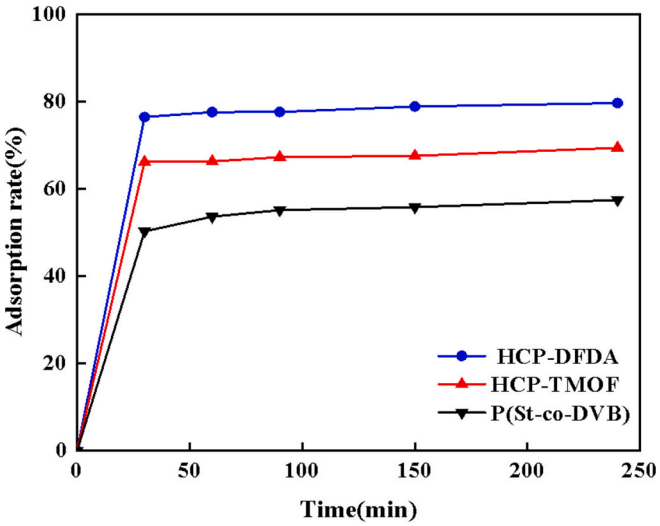

Fig. 7. Adsorption behavior of the adsorbents towards PCS in BSA solution.

3.2. Adsorption properties of the adsorbents towards uraemic toxins

PCS was used as the target toxin to evaluate the adsorption performance of various adsorbents towards PBUTs. An initial concentration of 25 mg L^{-1} PCS-BSA solution was prepared in a 40 gL^{-1} bovine serum albumin buffered solution via an external addition method. Fig. 7 depicts the adsorption rate curves of PCS by different adsorbents as a function of time. Evidently, the adsorption rate of PCS initially increased rapidly and then plateaued as the contact time lengthened. The experimental findings demonstrated that HCP-DFDA exhibited the optimal adsorption performance for PCS, with the adsorption rate reaching up to 78.8 % after 2 h. HCP-TMOF adsorbents also showed higher adsorption rates for PCS than P(St-co-DVB).

To directly verify the contribution of tertiary amine groups in the HCP-DFDA adsorbent for PBUT adsorption, we conducted oxidative modification treatment on the resin and compared the adsorption rates of PCS before and after modification. The experimental results are presented in Figure _S2. Under identical conditions, the adsorption rate of PCS by the oxidized HCP-DFDA decreased to 69.8 %, which was approximately 10 percentage points lower than that of unmodified adsorbent. In contrast, for the HCP-TMOF resin, the adsorption rates of PCS before and after the oxidation modification were 70.1 % and 69.9 %, respectively, showing no significant change. Through oxidation modification, the tertiary amine groups on the HCP-DFDA adsorbent were transformed into N-oxides (Figure _S1), exhibiting neutral zwitterionic characteristics, which result in negligible electrostatic interactions with the negatively charged PBUTs, thereby reducing the adsorbent's adsorption efficiency. Thus, it is evident that the tertiary amine groups on the HCP-DFDA adsorbent play a substantial role in the adsorption of PBUTs.

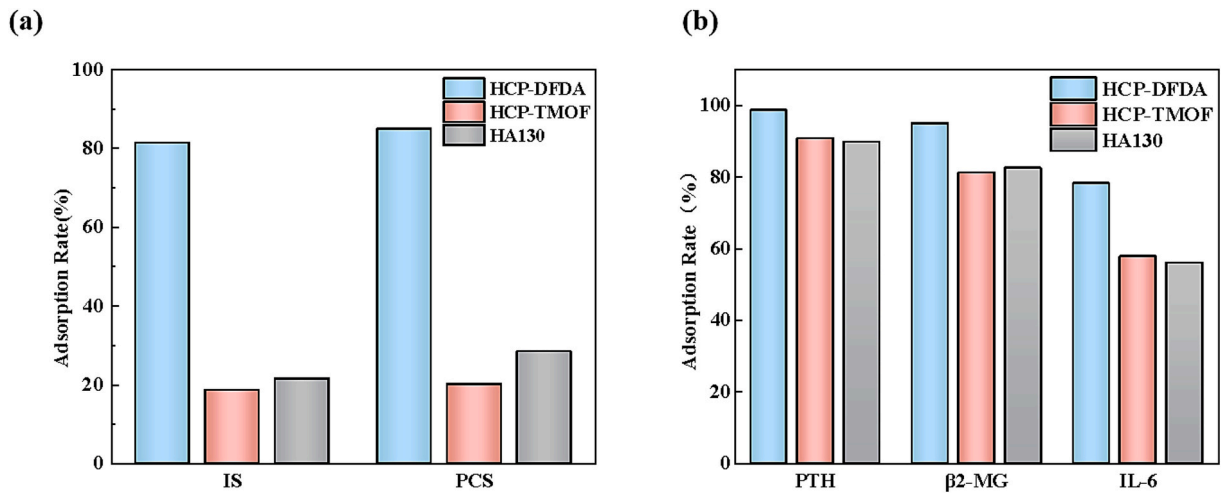

Fig. 8. Adsorption behavior of the adsorbents towards (a) PBUTs and (b) middle-macromolecular toxins in human plasma.

To further investigate the potential application of the hyper-crosslinked modified adsorbents in hemoperfusion for uremia treatment, we selected several common uremic toxins as target toxins, including medium- to large-molecular-weight toxins (PTH, β2-MG, and IL-6), and PBUTs (IS and PCS). We aimed to evaluate the adsorption performances of different adsorbents by using human plasma to closely mimic the clinical hemoperfusion conditions. Fig. 8 illustrates the adsorption rates of HCP-DFDA, HCP-TMOF, and the commercially available hemoperfusion adsorbent HA130 for various uremic toxins. As shown in Fig. 8 (a), after 2 h of contact adsorption, HCP-DFDA exhibited adsorption rates of 81.3 % and 84.9 % for IS and PCS, respectively. These rates were significantly higher than those of the HCP-TMOF and HA130 adsorbents. Fig. 8(b) displayed the adsorption rates of different adsorbents for medium- to large-molecular-weight toxins. After 2 h of adsorption in a plasma environment, the adsorption rates of HCP-TMOF for PTH, β2-MG, and IL-6 were 90.7 %, 81.2 %, and 57.8 %, respectively. These values were comparable to those of the commercial HA130 adsorbent (PTH: 89.7 %; β2-MG: 82.5 %; IL-6: 56.0 %). The HCP-DFDA adsorbent achieved adsorption rates of 98.6 %, 94.9 %, and 78.2 % for PTH, β2-MG, and IL-6, respectively, which were significantly better than those of the HCP-TMOF and HA130 adsorbents. These findings indicated that the HCP-DFDA adsorbent demonstrated excellent adsorption performance

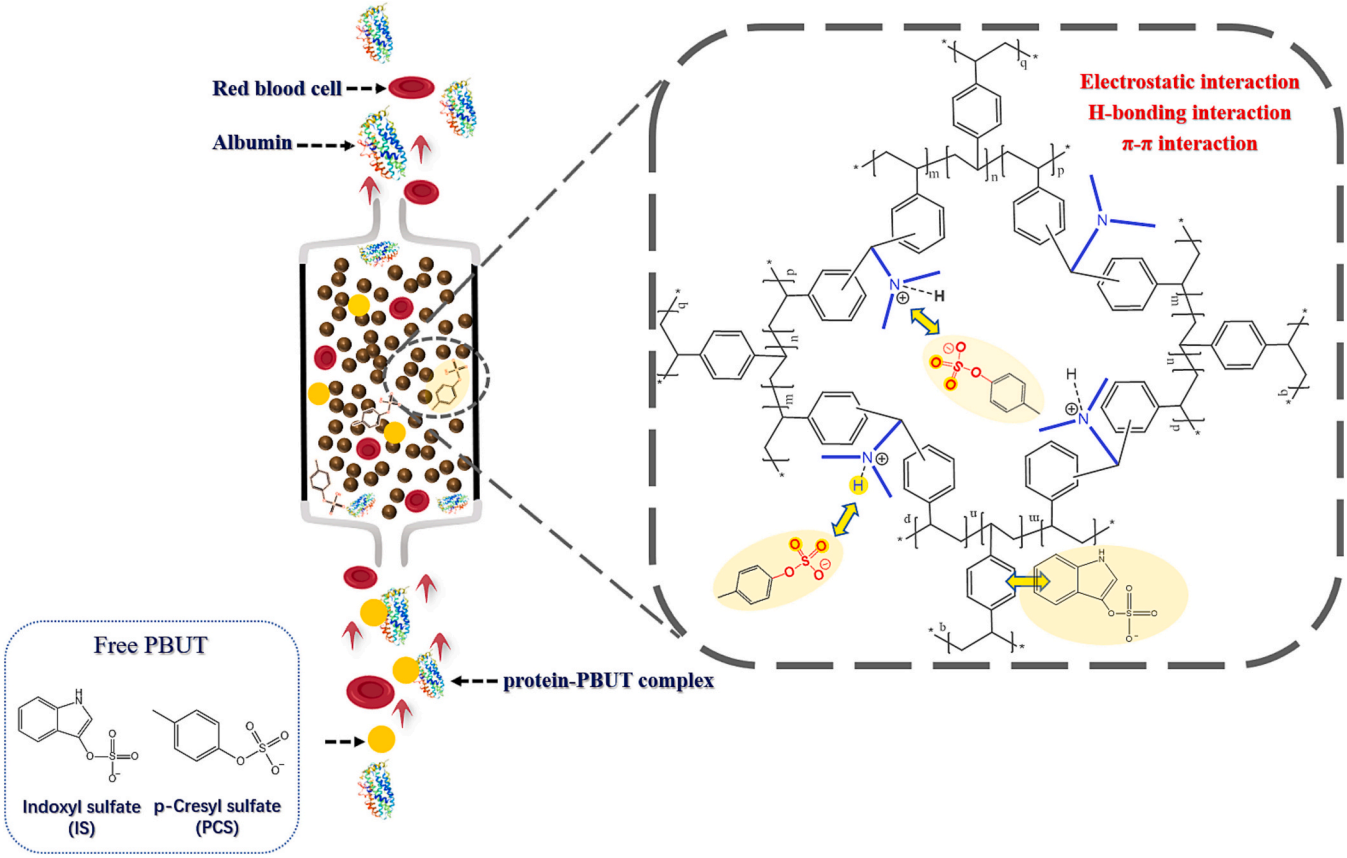

Fig. 9. Illustration of the adsorption mechanism of PBUTs by using HCP-DFDA.

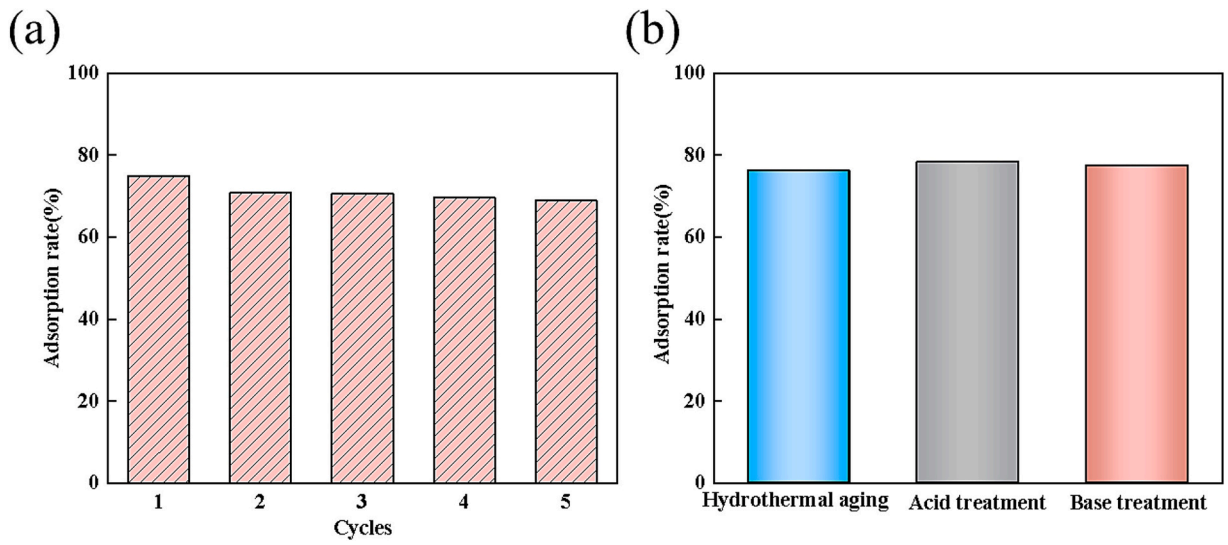

Fig. 10. (a) The recycling performance of HCP-DFDA in five recycles of PCS adsorption-desorption procedure; (b) Comparative adsorption rates of PCS by the HCP adsorbents HCP-DFDA that has undergone hydrothermal aging, acid treatment and base treatment.

for both PBUTs and medium- to large-molecular-weight toxins.

The excellent adsorption performance of HCP-DFDA for both medium- and large-molecule toxins and PBUTs can be mainly ascribed to its unique chemical structure and pore morphology. Similar to the HCP-TMOF and HA130 adsorbents, HCP-DFDA had hydrophobic benzene rings in its skeleton structure. This feature was beneficial for adsorbing lipid-soluble medium- and large-molecule toxins with aromatic rings in the blood through hydrophobic interactions or π-π interactions. Generally, the pore size of an adsorbent has a crucial influence on its adsorption performance for medium- and large-molecule toxins; larger pore sizes are more favorable for enhancing the adsorption of such toxins. According to the experimental results presented in Table 1 and Fig. 6, the average pore sizes of HCP-DFDA and HCP-TMOF were 5.42 nm and 8.71 nm, respectively. Although the average pore size of HCP-DFDA was considerably smaller than that of HCP-TMOF, its adsorption performance for medium- and large-molecule toxins was better. This can be primarily ascribed to the higher specific surface area, the confined pore effect, and the presence of functional groups within the pores of HCP-DFDA. Moreover, the contribution of the pore structures on the external surface of the adsorbents cannot be neglected. As shown in the SEM images in Fig. 5, in comparison with HCP-TMOF, HCP-DFDA exhibited more prominent and larger pore structures on its outer surface. These pore structures facilitated the rapid entry of medium- and large-molecule toxins into the interior of the adsorbent and their transportation to adsorption sites, thus enhancing the adsorption performance.

For the adsorption of PBUTs, HCP-DFDA also demonstrated significantly superior adsorption performance, which can be attributed to the tertiary amine groups in its structure. Generally, PBUTs in uremic patients are firmly bound to plasma proteins (such as albumin) to form protein-PBUTs toxin complexes. This binding behavior leads to a low concentration of free PBUTs in the bloodstream, rendering them challenging to eliminate. The nitrogen atoms within the tertiary amine groups possess lone pair electrons, which readily accept protons and form positively charged quaternary ammonium ions. These ions can establish strong electrostatic attractions with PBUTs that contain negatively charged groups (such as IS, PCS, etc.). Moreover, the hydrogen atoms on the quaternary ammonium ions can act as hydrogen bond donors. Conversely, the oxygen atoms in the negatively charged groups of PBUTs can function as hydrogen bond acceptors, forming hydrogen bonds that strengthen the interaction between the adsorbent and PBUTs. Consequently, under the combined influence of the pore structures, π-π interactions, and the interactions between the functional groups of the adsorbent and toxin molecules, HCP-DFDA was able to achieve efficient adsorption of free PBUT molecules. The uptake of PBUTs disrupted the adsorption equilibrium of the protein-PBUTs toxin complex, causing the PBUTs to continuously dissociate from the complex, and ultimately achieving an optimal removal effect. The adsorption mechanism is illustrated in Fig. 9.

3.3. Recyclability and stability of HCP-DFDA

To investigate the recyclability of the HCP-DFDA adsorbent, a series of five consecutive adsorption - desorption cycles were conducted, and the PCS adsorption performance of the repeatedly regenerated adsorbent was evaluated. The results are shown in Fig. 10(a). After five cycles of repeated use, the adsorption rate of HCP-DFDA exhibited a gradual decline from 75.03 % to 68.95 %, with only a marginal reduction of 6.08 % across the cycles, indicating that HCP-DFDA exhibits favorable recyclability and consistent performance over multiple cycles.

For the stability testing, the HCP-DFDA adsorbent underwent rigorous testing protocols, including exposure to high-temperature conditions and immersion in both strongly acidic and alkaline solutions, to evaluate its robustness under extreme environmental conditions. The experimental results are depicted in Fig. 10(b). As can be seen from the results, the adsorption rates of the HCP-DFDA adsorbent after hydrothermal aging, acid treatment and base treatment were 76.09 %, 78.35 %, and 77.38 %, respectively. There was no significant decrease in the adsorption performance compared to that of the untreated HCP-DFDA adsorbent. The HCP-DFDA adsorbent maintained stable adsorption performance after these rigorous treatments, thereby demonstrating its exceptional chemical stability and potential for practical applications in diverse environmental conditions.

3.4. Adsorption isotherms and adsorption kinetics towards PBUTs in PBS environment

To further understand the adsorption characteristics of the HCP-DFDA adsorbent for PBUTs, PCS and IS were used as model molecules to investigate the adsorption behavior of the adsorbent in the PBS environment. Adsorption isotherms were used to estimate the interaction mechanisms between HCP-DFDA and PBUT at a constant temperature. As shown in Fig. 11(a), the adsorption capacity of HCP-DFDA towards PCS/IS exhibits a positive correlation with the equilibrium

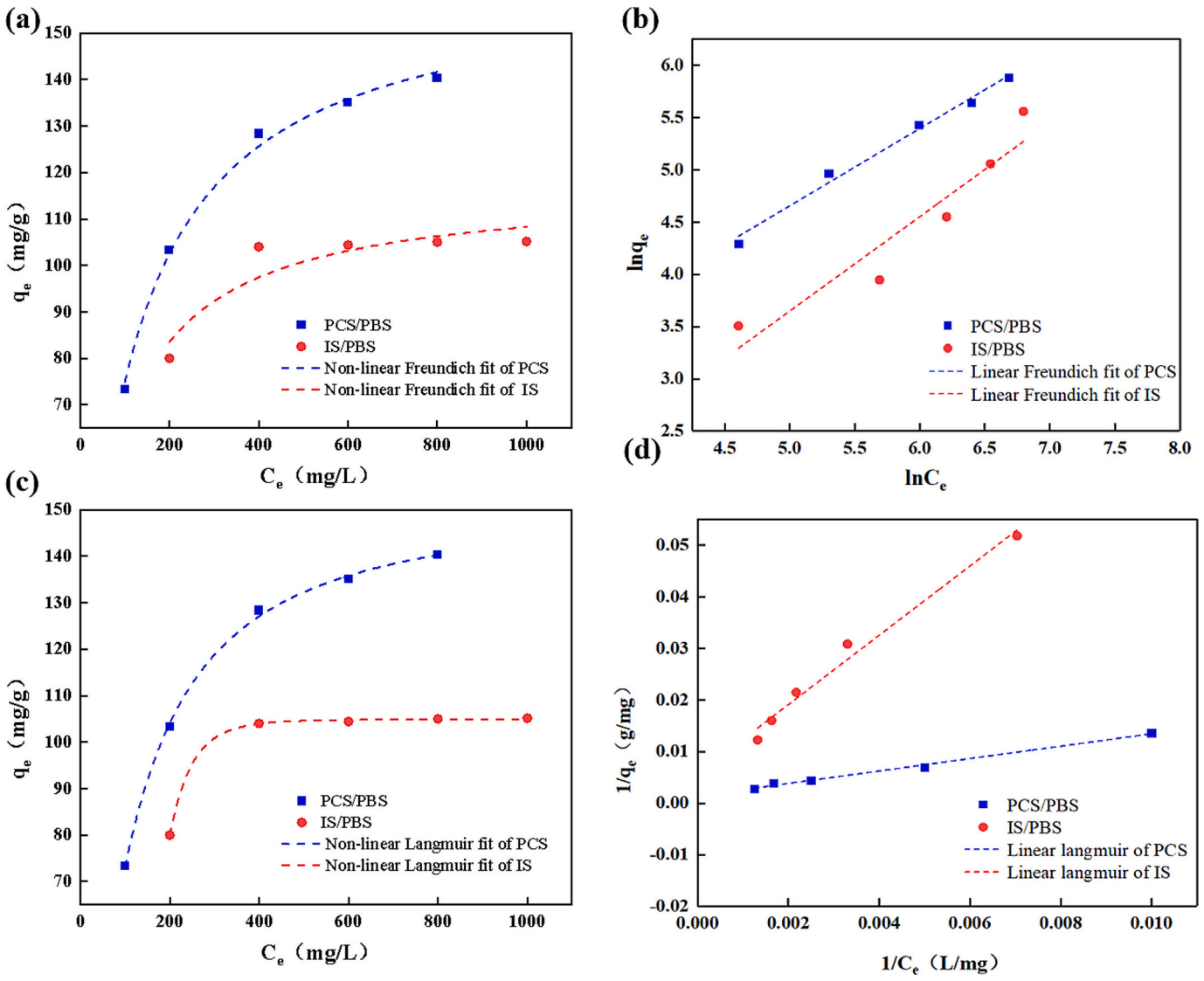

Fig. 11. PCS/IS adsorption isotherms of HCP-DFDA: (a) nonlinear Freundlich, (b) linear Freundlich, (c) nonlinear Langmuir, and (d) linear Langmuir model fitting plots.

concentration. This relationship can be attributed to the fact that an increase in toxin concentrations enhance the driving force that facilitating the mass transfer from the free state to the adsorbed phase. The experimental data were fitted via linear and nonlinear Langmuir (Eqs. (6), (7)) and Freundlich (Eqs. (8), (9)) isothermal adsorption models [41,42].

The linear and nonlinear Langmuir isothermal adsorption formulas are as follows:

$$\text{Linear Langmuir model}: {}^{1}/_{q_e} = {}^{1}/_{K_L q_m C_e} + {}^{1}/_{q_m} \quad (6)$$

$$\text{Non-linear Langmuir model}: q_e = q_m K_L C_e / (1 + K_L C_e) \quad (7)$$

The linear and nonlinear Freundlich isothermal adsorption formulas are as follows:

$$\text{Linear Freundlich model}: \ln(q_e) = {}^{1}/_{n} \ln(C_e) + \ln(K_F) \quad (8)$$

$$\text{Non-linear Freundlich model}: q_e = K_F C_e^{1/n} \quad (9)$$

Where q_e (mg·g^{-1}) is the sorption amount after equilibrium is achieved, and C_e (mg·L^{-1}) is the equilibrium concentration. The maximum adsorption capacity (q_m) (mg·g^{-1}) is calculated using the Langmuir model, and K_L (L/mg) denotes the Langmuir isotherm constant. Additionally, K_F (mg·g^{-1}) (L·mg^{-1})$^{1/n}$) and n are the Freundlich constants. C_0

Table 2
Adsorption isotherm parameters of HCP-DFDA towards PCS/IS.

PBUT	Fitting method	Langmuir			Freundlich		
		q_m(mg/g)	K_L/(L·mg^{-1})	R^2	K_F/(mg·g^{-1})(L·mg^{-1})$^{1/n}$	1/n	R^2
PCS	Linear	169.9301	0.0118	0.9966	2.6069	0.2393	0.9946
	Nonlinear	151.9953	0.0086	0.9945	2.1088	0.2826	0.9886
IS	Linear	120.0563	0.01724	0.9956	30.3044	0.1229	0.9231
	Nonlinear	104.9358	0.01252	0.9946	30.4147	0.1478	0.9030

Table 3
Adsorption kinetic parameters of HCP-DFDA towards PCS/IS.

PBUT	$q_{e,exp}$/(mg·g^{-1})	Pseudo-1st-order			Pseudo-2nd-order		
		$q_{e,cal,1}$/(mg·g^{-1})	k_1/min^{-1}	R^2	$q_{e,cal,2}$/(mg·g^{-1})	K_2/(g^{-1}·mg^{-1}·min^{-1})	R^2
PCS	58.59	17.26	0.0051	0.9471	57.74	0.0007	0.9998
IS	35.42	2.20	0.0036	0.9436	34.95	0.0064	0.9999

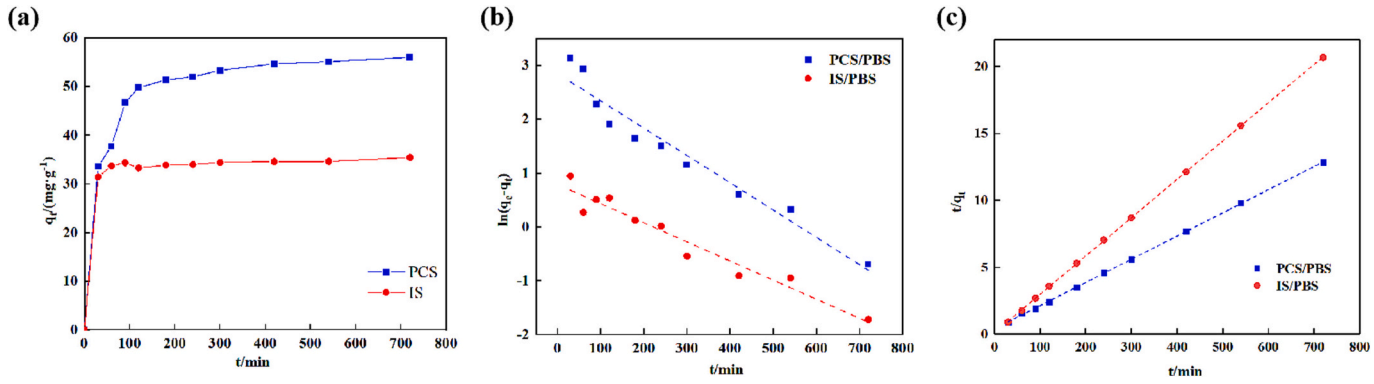

Fig. 12. (a) The uptake of PCS/IS versus time in PBS environment, (b) Pseudo-first-order and (c) Pseudo-second-order isotherm models for PCS/IS adsorption on HCP-DFDA.

(mg·L^{-1}) signifies the initial PBUT concentration, which serves as a crucial characteristic in the Langmuir isotherm [43,44].

Table 2 shows the fitting results. The Langmuir isotherm displays higher R^2 values than the Freundlich isotherm. This indicated that the adsorption equilibrium data of HCP-DFDA towards PCS/IS was more accurately described by the Langmuir equation, suggesting that homogeneous monolayer adsorption was the dominant adsorption mechanism [44]. The maximum adsorption capacities of PCS and IS, as calculated by the Langmuir model, were 169.9301 mg·g^{-1} and 120.0563 mg·g^{-1}, respectively. Compared with other materials are shown in Table S3, such as activated carbon, polymeric membrane, fiber, and metal-organic frameworks, HCP-DFDA showed an obvious advantage in the specific adsorption of PBUTs [11,45–48].

This study further explored the changes in the equilibrium adsorption capacity of the HCP-DFDA adsorbent for PCS at different reaction temperatures (298 K, 303 K, and 310 K). The experimental results are shown in Figure S3. Increasing the reaction temperature can effectively enhance the equilibrium adsorption capacity of HCP-DFDA for PCS. This is attributed to the fact that an increase in temperature is capable of strengthening the binding energy between the HCP-DFDA adsorbent and the PCS, thereby facilitating the forward progression of the adsorption reaction.

The relevant adsorption thermodynamic parameters calculated through the Clausius-Clapeyron, Gibbs, and Gibbs-Helmholtz equations [49] are listed in Table_S3 As shown in the table, under various temperature conditions, the Gibbs free energy change (ΔG) values are all negative, indicating that the adsorption process was spontaneous. The enthalpy change (ΔH) and the entropy change (ΔS) are in the ranges of 234.53–269.32 kJ/mol and 62.65–70.20 J/mol·K, respectively. The ΔH values are all positive, indicating that the adsorption process of PCS by HCP-DFDA was an endothermic reaction involving chemical adsorption. The ΔS value was also positive, suggesting an increase in the degree of disorder at the solid-liquid interface and the irreversibility of the adsorption process. In conclusion, the adsorption process of PCS by HCP-DFDA was a spontaneous endothermic process, and under the experimental conditions, the adsorption reaction is irreversible.

3.5. Adsorption kinetics towards PBUTs in the PBS environment

The kinetic rates were modeled using the pseudo-first-order Eq. (10) and pseudo-second-order Eq. (11) to further understand the adsorption mechanisms [50], and the fitting results were summarized in Table 3.

$$\ln(q_e - q_t) = \ln q_{e,cal,1} - k_1 t \tag{10}$$

$$t/q_t = 1/k_2 q^2_{e,cal,2} + t/q_{e,cal,2} \tag{11}$$

where q_e is the adsorbed amount of PCS/IS in the equilibrium, q_t is the adsorption quantity of PCS/IS at time t (mg·g^{-1}), k_1 (min^{-1}) is the quasi-first-order equation rate constant, and k_2 (g·mg^{-1}·min^{-1}) is the quasi-second-order rate constant.

Fig. 12(a) illustrates the time-dependent adsorption curves of PCS and IS by HCP-DFDA. The experimental results indicated that the adsorption process of these PBUTs had a characteristic of "rapid adsorption, slow equilibrium." Surface adsorption and solute diffusion played crucial roles throughout this process. In the first hour, the large specific surface area and well-developed microporous structure of the adsorbents provided numerous available binding sites. Simultaneously, the high PCS concentration in the solution created a significant concentration gradient, thereby facilitating a rapid initial adsorption rate. As the experiment progressed, the surface adsorption sites gradually became saturated, resulting in a decrease in the adsorption rate. Ultimately, when most of the microporous adsorption sites were occupied or the toxin concentration gradient could no longer overcome the mass-transfer limitations, the adsorption process reached equilibrium. Under these conditions, the equilibrium adsorption capacities of HCP-DFDA for PCS and IS were 58.59 mg·g^{-1} and 35.42 mg·g^{-1}, respectively.

Adsorption kinetic data were simulated and analyzed using the pseudo-first-order and pseudo-second-order kinetic equations. The corresponding linear fitting curves are shown in Fig. 12(b-c), and the relevant adsorption kinetic parameters derived from the calculations are listed in Table 3. According to Table 3, a higher correlation coefficient ($R^2 > 0.999$) was obtained for the pseudo-second-order model, which indicated that the capture processes of PCS and IS were dominated by chemisorption. Additionally, the equilibrium adsorption capacities of HCP-DFDA for PCS and IS, calculated using the pseudo-second-order kinetic model, were 57.74 mg·g^{-1} and 34.95 mg·g^{-1}, respectively. These values were close to the experimentally determined equilibrium adsorption capacities.

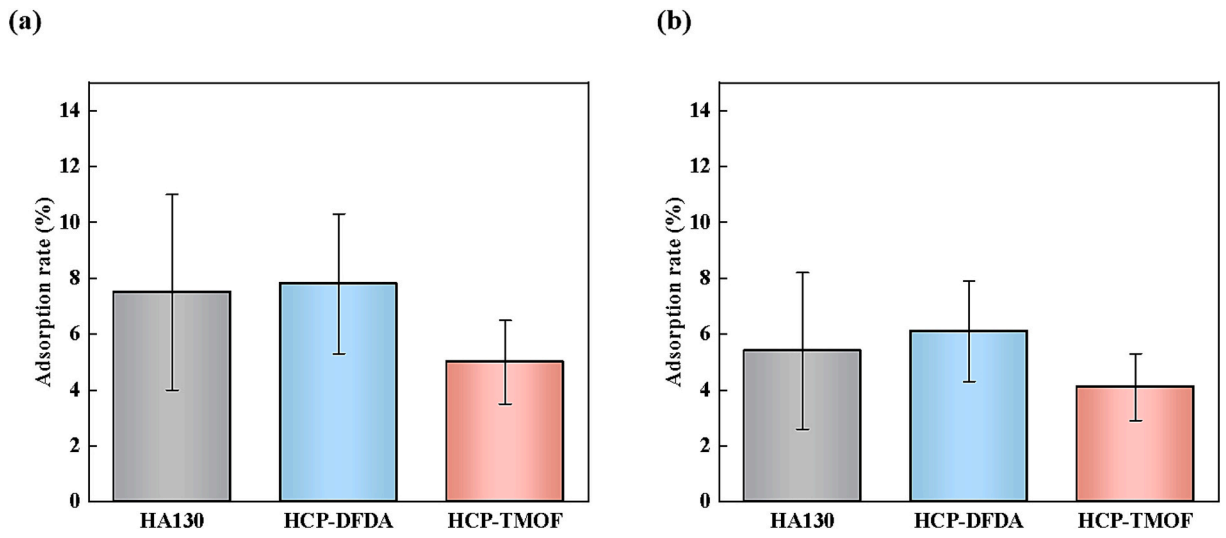

Fig. 13. Calculated adsorption rates of (a) albumin and (b) total protein from human plasma (adsorption time: 2 h). All values are expressed as the means ± SDs (n = 3).

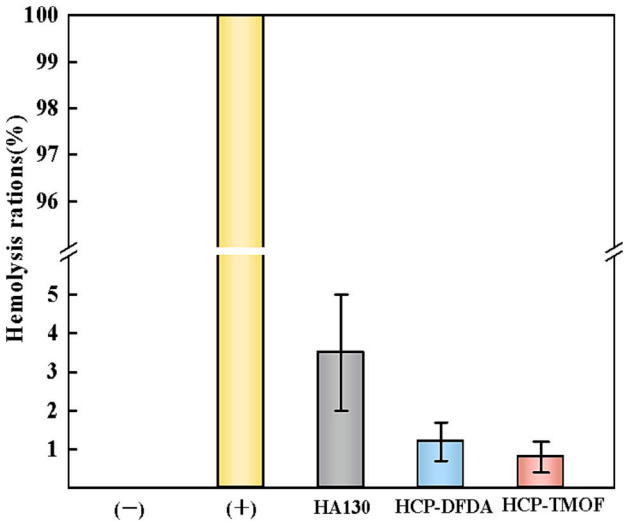

Fig. 14. Haemolysis ratios of the controls and adsorbents. Haemolysis test: (+) deionized water and (−) PBS solution. The data are expressed as the means ± SDs of three independent measurements.

3.6. Haemocompatibility of the adsorbents

Blood compatibility is a critical factor for materials intended for direct blood contact. To comprehensively evaluate the blood compatibility of the adsorbents, protein adsorption, hemolysis assays, and recalcification coagulation time measurements were employed [51].

Initially, the adsorption behavior of human plasma albumin and total proteins onto the adsorbents was investigated, with results presented in Fig. 13. The total protein adsorption rates for HCP-DFDA, HCP-TMOF, and HA130 were 6.1 ± 1.8 %, 4.1 ± 1.2 % and 5.4 ± 2.8 %, respectively. Statistical analysis revealed no significant difference in total protein adsorption among the HCP-DFDA group, HCP-TMOF group and the control group. Similarly, albumin adsorption rates for HCP-DFDA, HCP-TMOF, and HA130 were 7.8 ± 2.5 %, 5.0 ± 1.5 %, and 7.5 ± 3.5 %, respectively, with no statistically significant differences observed between the HCP-DFDA group, HCP-TMOF group and the control group.

The protein adsorption performance on adsorbent surfaces is closely related to their physicochemical structures. The protein adsorption rates of HCP-DFDA and HCP-TMOF were comparable to those of the commercial HA130 resin, which can be attributed to the fact that all three adsorbents belong to the hypercrosslinked polystyrene macroporous adsorption resin family with similar surface chemical properties. Furthermore, the hydrophilic surface characteristics of these adsorbents effectively inhibited non-specific protein adsorption, thereby maintaining blood component integrity during clinical applications. These findings demonstrated that HCP-DFDA and HCP-TMOF hypercrosslinked adsorbents exhibited comparable protein resistance to the HA130 adsorbent, thereby preserving the normal physiological state of blood during clinical application and minimizing treatment-related risks.

When adsorbent materials interact with blood, their surfaces may induce erythrocyte membrane damage, triggering hemolytic reactions that release haemoglobin and other small molecular toxins harmful to vital organs. In this study, hemolysis assays were conducted to further evaluate the blood compatibility of the adsorbents. According to ISO 10993-5:2009 guidelines for the biological evaluation of medical devices, the hemolysis rate of biomaterials intended for blood contact must be less than 5 % to meet clinical requirements. The hemolysis rates of different adsorbents, negative control (phosphate-buffered saline), and positive control (deionized water) were compared, as shown in Fig. 14. The hemolysis rates of the HCP-DFDA and HCP-TMOF adsorbents were 1.2 ± 0.5 % and 0.8 ± 0.4 %, respectively, which were significantly lower than that of the HA130 adsorbent (3.5 ± 1.5 %). Both HCP-DFDA and HCP-TMOF demonstrated hemolysis rates well within the acceptable range, confirming their non-hemolytic properties.

The lower hemolysis rates of HCP-DFDA and HCP-TMOF compared to commercial HA resin were found to be associated with three critical factors: superior surface smoothness, lower ion exchange capacity, and neutral pH storage conditions. The adsorbents' highly smooth surfaces minimized mechanical friction with erythrocyte membranes and reduced shear stress-induced membrane disruption. Their low ion exchange capacity indicated lower surface charge density, mitigated electrostatic interactions that could damage cell membranes. Furthermore, the neutral pH of the storage solution for HCP-DFDA and HCP-TMOF maintained erythrocyte membrane protein stability by preventing acid/base-induced denaturation and osmotic imbalance.

The anticoagulant properties of the adsorbents were investigated using plasma recalcification time assays [52]. Experiments were performed following a method previously described in our research. Venous blood was collected from healthy rabbits, with glass beads serving as a positive control. In recalcification time experiments, sample incubation with plasma induced varying degrees of activation of coagulation factor

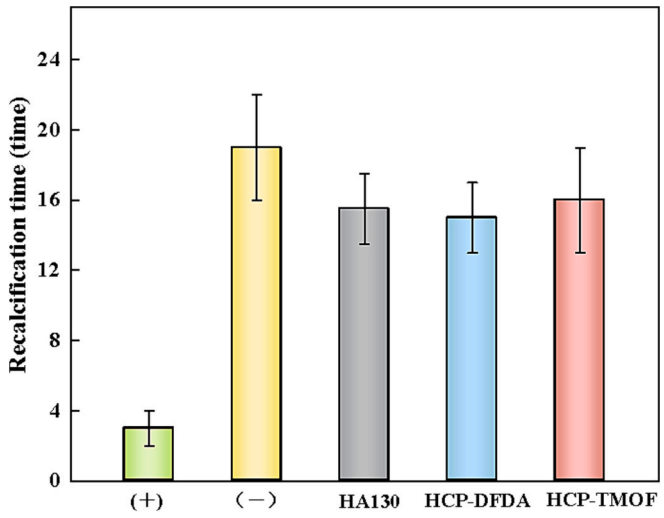

Fig. 15. Recalcification times of control samples and adsorbent materials. (+) hydrophilic glass beads and (−) blank tube. The data are expressed as the means ± SDs of three independent measurements.

XII (FXII) and platelets. When calcium chloride solution was added, the intrinsic coagulation pathway was initiated, converting plasma fibrinogen into fibrin and causing plasma solidification into a gel-like state. A shorter coagulation time indicated a higher extent of activation. As shown in Fig. 15, visible clot formation occurred within 4 min in the positive control samples. In contrast, the negative control group demonstrated a recalcification period of approximately 20 mins before clot formation. The recalcification time for HCP-DFDA, HCP-TMOF, and HA130 were 15 min, 16 min, and 15.5 min, respectively. These results indicated that both HCP-DFDA and HCP-TMOF exhibited anticoagulant properties comparable to the commercial HA130 adsorbent. The excellent anticoagulant properties of HCP-DFDA and HCP-TMOF are primarily attributed to their favorable hydrophilicity and good anti-protein adsorption performance, which collectively maintain blood component stability during clinical applications.

The in vitro haemocompatibility tests described above indicated that the hypercrosslinked adsorbents HCP-DFDA and HCP-TMOF exhibited low protein adsorption, low hemolysis rates, and excellent anticoagulant properties compared to commercial adsorbents. These attributes ensure that upon blood contact, these materials preserve the integrity of blood components without inducing excessive blood cell damage or coagulation responses, which is highly advantageous for whole blood perfusion applications.

4. Conclusions

In this study, a hypercrosslinked polystyrene porous adsorbent (HCP-DFDA) functionalized with tertiary amine groups was successfully synthesized. By using a functionalized small-molecule external crosslinker, this method simultaneously accomplished Friedel–Crafts post-crosslinking and surface functionalization of the pre-crosslinked polystyrene resin. The resulting HCP-DFDA adsorbent exhibited a smooth and flat external surface and a hierarchical crosslinked pore structure, achieving a specific surface area of 1030 m^2/g. Compared with the pre-crosslinked polystyrene resin P(St-co-DVB), HCP-DFDA demonstrated notable increases in total specific surface area and micropore content. The introduction of tertiary amine groups significantly enhanced its adsorption performance for PBUTs. Under plasma conditions, HCP-DFDA achieved adsorption efficiencies of 81.3 % for IS and 84.9 % for PCS, outperforming the non-functionalized HCP-TMOF and the commercial hemoperfusion adsorbent HA130. Furthermore, HCP-DFDA exhibited excellent adsorption capacities for medium- to large-molecular-weight toxins in blood, including PTH, β2-MG, and IL-6, surpassing those of HA130. In addition, the hypercrosslinked HCP-DFDA adsorbent displayed excellent blood compatibility comparable to the commercial HA130. In conclusion, HCP-DFDA is expected to serve as a promising new whole-blood hemoperfusion adsorbent for clinical uremia treatment.

CRediT authorship contribution statement

Lingyu Chen: Writing – review & editing, Writing – original draft. **Yunhong Liu:** Writing – review & editing, Conceptualization. **Xinyan Peng:** Writing – review & editing, Writing – original draft. **Yuelan Wei:** Methodology, Formal analysis. **Ke Shao:** Methodology.

Declaration of competing interest

The authors declare that they have no known competing financial interests or personal relationships that could have appeared to influence the work reported in this paper.

Acknowledgements

This work was financially supported by the National Natural Science Foundation of China (82100793), the Natural Science Foundation of Fujian Province, China (Grant Nos. 2020J05152 and 2020J05153) and the Ph.D. Research Start-up Fund Project of Quanzhou Normal University. We gratefully acknowledge Jafron Company for providing a performance evaluation system for the absorbents, including toxin adsorption tests and blood compatibility evaluations. The authors would like to express sincere gratitude to BSD Instrument Technology (Beijing) Co., Ltd. for providing complimentary BET testing services.

Appendix A. Supplementary data

Supplementary data to this article can be found online at https://doi.org/10.1016/j.reactfunctpolym.2025.106265.

Data availability

No data was used for the research described in the article.

References

[1] D. Pavlenko, D. Giasafaki, G. Charalambopoulou, E. van Geffen, K.G.F. Gerritsen, T. Steriotis, D. Stamatialis, Carbon adsorbents with dual porosity for efficient removal of uremic toxins and cytokines from human plasma, Sci. Rep. 7 (2017), https://doi.org/10.1038/s41598-017-15116-y.
[2] T. Ansari, M. Arslan, S. Manzoor, G. Yasmeen, Activated Carbon Based Ormosils for Abatement of Uremic Toxins from Blood Plasma Samples, Elsevier BV, 2024, https://doi.org/10.2139/ssrn.4685239 (accessed December 3, 2024).
[3] B. Koubaissy, J. Toufaily, Z. Yaseen, T.J. Daou, S. Jradi, T. Hamieh, Adsorption of uremic toxins over dealuminated zeolites, Adsorpt. Sci. Technol. 35 (2016) 3–19, https://doi.org/10.1177/0263617416666084.
[4] D. Bergé-Lefranc, H. Pizzala, J.L. Paillaud, O. Schäf, C. Vagner, P. Boulet, B. Kuchta, R. Denoyel, Adsorption of small uremic toxin molecules on MFI type zeolites from aqueous solution, Adsorption 14 (2008) 377–387, https://doi.org/10.1007/s10450-007-9093-6.
[5] V. Wernert, O. Schäf, H. Ghobarkar, R. Denoyel, Adsorption properties of zeolites for artificial kidney applications, Microporous Mesoporous Mater. 83 (2005) 101–113, https://doi.org/10.1016/j.micromeso.2005.03.018.
[6] Z. He, H. Lu, X. Jian, G. Li, D. Xiao, Q. Meng, J. Chen, C. Zhou, The efficacy of resin Hemoperfusion cartridge on inflammatory responses during adult cardiopulmonary bypass, Blood Purif. 51 (2021) 31–37, https://doi.org/10.1159/000514149.
[7] J. Chen, W. Han, R. Su, J. Chen, W. Zong, Y. Wang, W. Wang, G. Cheng, L. Ou, Y. Yu, Non-ionic macroporous polystyrene adsorbents for removal of serum toxins in liver failure by hemoperfusion, Artif. Cells Nanomed. Biotechnol. 45 (2016) 174–183, https://doi.org/10.3109/21691401.2016.1138494.
[8] M. Zhang, L. Li, L. Lei, K. Kang, C. Xiao, Effectively decontaminating protein-bound uremic toxins in human serum albumin using cationic metal–organic frameworks, ACS Appl. Mater. Interfaces 14 (2022) 55354–55364, https://doi.org/10.1021/acsami.2c15864.

[9] S. Kato, K. Otake, H. Chen, I. Akpinar, C.T. Buru, T. Islamoglu, R.Q. Snurr, O. K. Farha, Zirconium-based metal–organic frameworks for the removal of protein-bound uremic toxin from human serum albumin, J. Am. Chem. Soc. 141 (2019) 2568–2576, https://doi.org/10.1021/jacs.8b12525.
[10] Z. Chao, J. Li, W. Jiang, C. Zhang, J. Ji, X. Hua, L. Xu, L. Han, L. Jia, Hemocompatible MOF-decorated pollen hemoperfusion absorbents for rapid and highly efficient removal of protein-bound uremic toxins, Mater. Chem. Front. 5 (2021) 7617–7627, https://doi.org/10.1039/d1qm01071a.
[11] T. Chen, M. Wang, K. Tan, C. Chen, M. Li, C. Mao, Ibuprofen loaded into metal–organic framework shells coated on Fe3O4 nanoparticles for the removal of protein-bound uremic toxins in blood, ACS Appl. Nano Mater. 5 (2022) 5838–5846, https://doi.org/10.1021/acsanm.2c01026.
[12] T. Wang, W. Gu, L. Yu, X. Guo, J. Yang, X. Sun, J. Guan, L. Zhou, C. Wang, H. Yao, X. Zhang, G. Wang, MXene: an efficient hemoperfusion sorbent for the removal of uremic toxins, J. Mater. 9 (2023) 1129–1140, https://doi.org/10.1016/j.jmat.2023.06.010.
[13] S. Yamamoto, T. Ito, M. Sato, S. Goto, J.J. Kazama, F. Gejyo, I. Narita, Adsorption of protein-bound uremic toxins using activated carbon through direct Hemoperfusion in vitro, Blood Purif. 48 (2019) 215–222, https://doi.org/10.1159/000500014.
[14] E. Riccio, M. Cataldi, M. Minco, G. Argentino, R. Russo, S. Brancaccio, A. Memoli, L. Grumetto, L. Postiglione, B. Guida, B. Memoli, Evidence that p-cresol and IL-6 are adsorbed by the HFR cartridge: towards a new strategy to decrease systemic inflammation in dialyzed patients? PLoS One 9 (2014) e95811 https://doi.org/10.1371/journal.pone.0095811.
[15] G. Ankawi, W. Fan, D. Pomarè Montin, A. Lorenzin, M. Neri, C. Caprara, M. de Cal, C. Ronco, A new series of sorbent devices for multiple clinical purposes: current evidence and future directions, Blood Purif. 47 (2018) 94–100, https://doi.org/10.1159/000493523.
[16] D. Zhao, Y. Wang, Y. Wang, A. Jiang, N. Cao, Y. He, J. Wang, Z. Guo, W. Liu, W. Shi, L. Hao, J. Li, W. Li, C. Wang, J. Wang, H. Lin, W. Shi, L. Wang, H. Jiang, G. Ding, Y. Li, W. Hu, H. Yue, J. Liu, X. Yang, Y. Yang, G. Liu, H. Li, Y. Xiao, N. Wang, G. Jiang, G. Ma, J. Wang, Y. Li, R. Li, Q. Li, S. Sun, J. Jiao, C. Xi, G. Cai, X. Sun, X. Chen, Randomized control study on Hemoperfusion combined with hemodialysis versus standard hemodialysis: effects on middle-molecular-weight toxins and uremic pruritus, Blood Purif. 51 (2022) 812–822, https://doi.org/10.1159/000525225.
[17] H. Wang, H. Jin, W. Cheng, X. Qin, Y. Luo, X. Liu, Y. Fu, G. Jiang, W. Lu, C. Jin, M. Pennington, Cost-effectiveness analysis of hemodialysis plus hemoperfusion versus hemodialysis alone in adult patients with end-stage renal disease in China, Ann. Transl. Med. 9 (2021) 1133, https://doi.org/10.21037/atm-21-1100.
[18] R. Hayama, T. Koyama, T. Matsushita, K. Hatano, K. Matsuoka, Preparation of functional monomers as precursors of bioprobes from a common styrene derivative and polymer synthesis, Molecules 23 (2018) 2875, https://doi.org/10.3390/molecules23112875.
[19] A. Koler, I. Pulko, P. Krajnc, Post polymerisation Hypercrosslinking with emulsion templating for hierarchical and multi-level porous polymers, Acta Chim. Slov. 67 (2020) 349–360, https://doi.org/10.17344/acsi.2020.5901.
[20] B. Li, R. Gong, W. Wang, X. Huang, W. Zhang, H. Li, C. Hu, B. Tan, A new strategy to microporous polymers: knitting rigid aromatic building blocks by external cross-linker, Macromolecules 44 (2011) 2410–2414, https://doi.org/10.1021/ma200630s.
[21] J.-H. Ahn, J.-E. Jang, C.-G. Oh, S.-K. Ihm, J. Cortez, D.C. Sherrington, Rapid generation and control of microporosity, bimodal pore size distribution, and surface area in Davankov-type hyper-cross-linked resins, Macromolecules 39 (2005) 627–632, https://doi.org/10.1021/ma051152n.
[22] F. Maya, F. Svec, A new approach to the preparation of large surface area poly (styrene-co-divinylbenzene) monoliths via knitting of loose chains using external crosslinkers and application of these monolithic columns for separation of small molecules, Polymer 55 (2014) 340–346, https://doi.org/10.1016/j.polymer.2013.08.018.
[23] P. Pączkowski, B. Gawdzik, Studies on preparation, Characterization and application of porous functionalized glycidyl methacrylate-based microspheres, Materials 14 (2021) 1438, https://doi.org/10.3390/ma14061438.
[24] M. Maciejewska, M. Grochowicz, Synthesis and thermal characterization of porous polymeric microspheres functionalized with thiol groups, J. Therm. Anal. Calorim. 148 (2023) 4195–4210, https://doi.org/10.1007/s10973-023-11972-1.
[25] Y. Luo, Y. Mei, Y. Xu, K. Huang, Hyper-crosslinked porous organic nanomaterials: structure-oriented design and catalytic applications, Nanomaterials 13 (2023) 2514, https://doi.org/10.3390/nano13182514.
[26] Q. Zhou, Z. Li, C. Shuang, A. Li, M. Zhang, M. Wang, Efficient removal of tetracycline by reusable magnetic microspheres with a high surface area, Chem. Eng. J. 210 (2012) 350–356, https://doi.org/10.1016/j.cej.2012.08.081.
[27] M. Errahali, G. Gatti, L. Tei, G. Paul, G.A. Rolla, L. Canti, A. Fraccarollo, M. Cossi, A. Comotti, P. Sozzani, L. Marchese, Microporous hyper-cross-linked aromatic polymers designed for methane and carbon dioxide adsorption, J. Phys. Chem. C 118 (2014) 28699–28710, https://doi.org/10.1021/jp5096695.
[28] B.C. Pan, Y. Xiong, A.M. Li, J.L. Chen, Q.X. Zhang, X.Y. Jin, Adsorption of aromatic acids on an aminated hypercrosslinked macroporous polymer, React. Funct. Polym. 53 (2002) 63–72, https://doi.org/10.1016/s1381-5148(02)00123-2.
[29] M. Ghafari, Y. Cui, A. Alali, J.D. Atkinson, Phenol adsorption and desorption with physically and chemically tailored porous polymers: mechanistic variability associated with hyper-cross-linking and amination, J. Hazard. Mater. 361 (2019) 162–168, https://doi.org/10.1016/j.jhazmat.2018.08.068.
[30] B. Díez-Buitrago, F.J. Fernández-SanArgimiro, J. Lorenzo, N. Briz, V. Pavlov, Modification of chlorosulfonated polystyrene substrates for bioanalytical applications, Mater. Sci. Eng. C 112 (2020) 110912, https://doi.org/10.1016/j.msec.2020.110912.
[31] Y. Gan, G. Chen, Y. Sang, F. Zhou, R. Man, J. Huang, Oxygen-rich hyper-cross-linked polymers with hierarchical porosity for aniline adsorption, Chem. Eng. J. 368 (2019) 29–36, https://doi.org/10.1016/j.cej.2019.02.164.
[32] J. Jung, H. Choi, S. Hong, S.J. Yoon, T.-H. Kim, J.Y. Lee, Y.T. Hong, S. So, Surface-initiated ATRP of glycidyl methacrylate in the presence of divinylbenzene on porous polystyrene-based resins for boron adsorption, Desalination 473 (2020) 114166, https://doi.org/10.1016/j.desal.2019.114166.
[33] D. Pei, X. Wu, Y. Liu, T. Huo, D. Di, M. Guo, L. Zhao, B. Wang, Different ionic liquid modified hypercrosslinked polystyrene resin for purification of catechins from aqueous solution, Colloids Surf. A Physicochem. Eng. Asp. 509 (2016) 158–165, https://doi.org/10.1016/j.colsurfa.2016.08.071.
[34] Y. Liu, X. Peng, Multi-functional Hypercrosslinked polystyrene as high-performance adsorbents for artificial liver blood purification, Front. Chem. 9 (2022), https://doi.org/10.3389/fchem.2021.789814.
[35] R. Tank, D.C. Gupta, Modification of styrene-divinyl benzene copolymers using monoacrylates as ter-monomer, J. Porous. Mater. 16 (2008) 387–392, https://doi.org/10.1007/s10934-008-9211-1.
[36] J. Manono, P.A. Marzilli, F.R. Fronczek, L.G. Marzilli, New porphyrins bearing Pyridyl peripheral groups linked by secondary or tertiary sulfonamide groups: synthesis and structural characterization, Inorg. Chem. 48 (2009) 5626–5635, https://doi.org/10.1021/ic900600z.
[37] S. Hofmann, Auger- and X-Ray Photoelectron Spectroscopy in Materials Science: A User-Oriented Guide, Springer Science & Business Media, 2012.
[38] T. Yusuke, K. Yamauchi, T. Mitsunaga, Phenolic Compounds Related to Heartwood Coloration of Millettia Pendula, Springer Science and Business Media LLC, 2024, https://doi.org/10.21203/rs.3.rs-4465855/v1 (accessed December 4, 2024.
[39] M. Thommes, Physisorption of gases, with special reference to the evaluation of surface area and pore size distribution (IUPAC technical report), Chem. Int. 38 (2016) 25, https://doi.org/10.1515/ci-2016-0119.
[40] K.W. Stahlfeld, E.L. Belmont, BET and Kelvin analyses by thermogravimetric desorption, Langmuir 39 (2023) 8814–8823, https://doi.org/10.1021/acs.langmuir.3c00854.
[41] K.Y. Foo, B.H. Hameed, Insights into the modeling of adsorption isotherm systems, Chem. Eng. J. 156 (2010) 2–10, https://doi.org/10.1016/j.cej.2009.09.013.
[42] I.Y. Erwa, O. Ishag, O. Alrefaeï, I. Hassan, Nonlinear fitting for estimation of adsorption equilibrium, kinetic and thermodynamic parameters of methylene blue onto activated carbon, J. Turk. Chem. Soc. A: Chem. 9 (2022) 67–84, https://doi.org/10.18596/jotcsa.904311.
[43] V. Wernert, O. Schäf, V. Faure, P. Brunet, L. Dou, Y. Berland, P. Boulet, B. Kuchta, R. Denoyel, Adsorption of the uremic toxin p-cresol onto hemodialysis membranes and microporous adsorbent zeolite silicalite, J. Biotechnol. 123 (2006) 164–173, https://doi.org/10.1016/j.jbiotec.2005.11.009.
[44] Z. Liu, Z. Wang, W. Gan, S. Liu, J. Zhang, Z. Ran, C. Wu, C. Hu, D. Wang, T. Chen, G. Li, Computational and experimental investigation of the selective adsorption of indium/Iron ions by the epigallocatechin Gallate monomer, Materials 15 (2022) 8251, https://doi.org/10.3390/ma15228251.
[45] N. Cai, Q. Li, J. Zhang, T. Xu, W. Zhao, J. Yang, L. Zhang, Antifouling zwitterionic hydrogel coating improves hemocompatibility of activated carbon hemoadsorbent, J. Colloid Interface Sci. 503 (2017) 168–177, https://doi.org/10.1016/j.jcis.2017.04.024.
[46] M. Sternkopf, T. Speer, C. Göttsch, V. Jankowski, J. Jankowski, H. Noels, P1101A bifunctional adsorber particle for the removal of hydrophobic uremic toxins from whole blood of renal failure patients, Nephrol. Dial. Transplant. 35 (2020), https://doi.org/10.1093/ndt/gfaa142.p1101.
[47] M.S.L. Tijink, M. Wester, G. Glorieux, K.G.F. Gerritsen, J. Sun, P.C. Swart, Z. Borneman, M. Wessling, R. Vanholder, J.A. Joles, D. Stamatialis, Mixed matrix hollow fiber membranes for removal of protein-bound toxins from human plasma, Biomaterials 34 (2013) 7819–7828, https://doi.org/10.1016/j.biomaterials.2013.07.008.
[48] H. Cuchiaro, J. Thai, N. Schaffner, R.R. Tuttle, M. Reynolds, Exploring the parameter space of p-Cresyl sulfate adsorption in metal–organic frameworks, ACS Appl. Mater. Interfaces 12 (2020) 22572–22580, https://doi.org/10.1021/acsami.0c04203.
[49] S. Liu, Z. Wang, M. He, J. Zhu, Preparation of 6-amino-N-hydroxyhexanamide-modified porous chelating resin for adsorption of heavy metal ions, Polymers 16 (2024) 1966, https://doi.org/10.3390/polym16141966.
[50] Q. Li, W. Zhao, H. Guo, J. Yang, J. Zhang, M. Liu, T. Xu, Y. Chen, L. Zhang, Metal–organic framework traps with record-high bilirubin removal capacity for hemoperfusion therapy, ACS Appl. Mater. Interfaces 12 (2020) 25546–25556, https://doi.org/10.1021/acsami.0c03859.
[51] M. Weber, H. Steinle, S. Golombek, L. Hann, C. Schlensak, H.P. Wendel, M. Avci-Adali, Blood-contacting biomaterials: in vitro evaluation of the hemocompatibility, Front. Bioeng. Biotechnol. 6 (2018), https://doi.org/10.3389/fbioe.2018.00099.
[52] K. Ma, D. Yao, J. Chen, Y. Li, C. Zhao, G. Liang, Molecular synergistic strategy to fabricate bilirubin medical adsorbent material for hyperbilirubinemia hemoperfusion, Int. J. Polym. Mater. Polym. Biomater. 67 (2017) 727–738, https://doi.org/10.1080/00914037.2017.1376198.